Four-Degree-of-Freedom Control for Dual Active Flexbattery H-Bridge Converter

Ya Zhang, Marcel A. M. Hendrix, Jorge L. Duarte, Maurice G.L. Roes, and Elena A. Lomonova
Eindhoven University of Technology
Department of Electrical Engineering
P.O. Box 513, 5600MB Eindhoven, The Netherlands
ya.zhang@tue.nl

***Abstract*—This paper proposes a four-degree-of-freedom control method for a dual active Flexbattery H-Bridge converter, which operates similarly to dual-active-bridge converters. The Flexbattery pack is constructed from multiple modular units and each unit contains one voltage source, one inductor and four switches. Due to the cascaded structure of the pack, it is able to generate high-frequency square-waveform signals with tunable amplitudes and duty cycles. Distinct from the well-known unified triple-phase-shift approach, the proposed control method includes one additional degree of freedom. The tunable control variables become one voltage amplitude, two duty cycles, and the phase shift. By taking the third harmonic into account, the proposed four-degree-of-freedom control method further reduces the circulating current.**

***Index Terms*—Multiple modular units, H-Bridge converter, Flexbattery, dual-active-bridge, four-degree-of-freedom control.**

I. Introduction

The isolated-dual-active-bridge (IDAB) converter is attracting increasing attention in power electronics as an interface between different voltage sources. Its utilization can be found in applications of sustainable energy generation, storage and distribution, and electrical vehicles [1], [2]. Studies on its overall performance improvement show a continuous evolution. For instance, starting from the first-proposed conventional-phase-shift (CPS) modulation [3], the control scheme moved on to dual-phase-shift (DPS) control [4], followed by triple-phase-shift (TPS) discussed in [5], and the recent optimization control, based on TPS and soft switching techniques in [6].

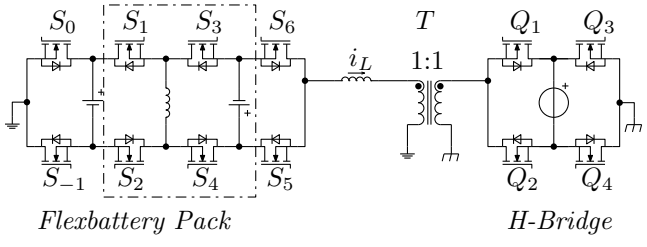

Fig. 1: An example of a single-unit Flexbattery H-Bridge converter. The basic Flexbattery unit is indicated in the dotted rectangular block.

As it is introduced in [7] and [8], a Flexbattery unit consists of four switches, an inductor and a battery cell (or a capacitor for an extended commutation cell [9], [10]), as indicated in the dotted rectangular box in Fig. 1. When connecting multiple units in a cascading way, a Flexbattery H-Bridge converter is obtained, as depicted in Fig. 2. The maximum voltage the Flexbattery can generate is equal to the sum of the battery voltage values in the Flexbattery pack. For instance, the two batteries of the Flexbattery pack in Fig. 1 are connected in series when the switches S_{-1}, S_1, S_3, S_5 are ON and the switches S_0, S_2, S_4, S_6 are OFF, and the maximum voltage is obtained accordingly. The voltage from the Flexbattery pack can be negative or positive, depending on the operation modes of the switches. Because the Flexbattery pack is a multilevel converter, the Flexbattery H-Bridge converter exhibits an additional degree of freedom for control compared to the traditional triple-phase-shift scheme applied in IDAB converters.

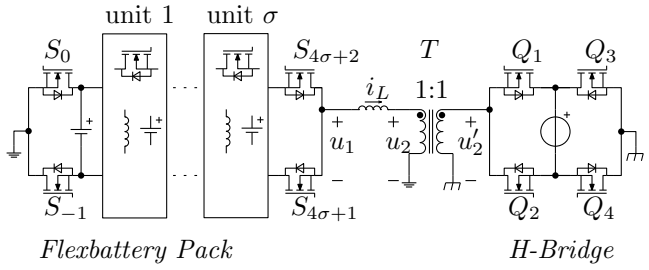

Fig. 2: General block diagram of the Flexbattery H-Bridge converter with σ extended commutation units.

II. Four-degree-of-freedom control for the Flexbattery H-Bridge converter

The Flexbattery H-Bridge converter consists of four parts: a Flexbattery pack comprising multiple units, an inductor, a transformer for galvanic isolation, and an H-bridge converter. The transformer T is assumed ideal, and therefore the schematic in Fig. 2 can be simplified to two voltage sources in series with an inductor, as shown in Fig. 3, where u_1 denotes the alternate voltage from the Flexbattery pack side, and u_2 refers to the voltage as imposed by the H-Bridge through the isolation transformer. The transformer primary-to-secondary transfer ratio has been already taken into account. The waveforms of the primary (u_1) and secondary

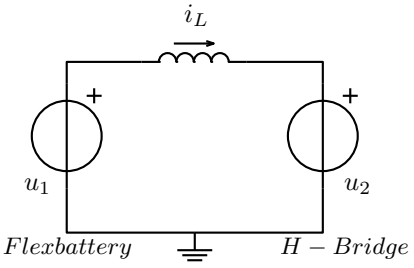

Fig. 3: Simplified circuit referred to the Flexbattery pack side.

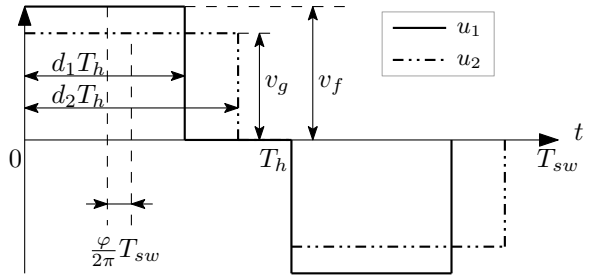

Fig. 4: Voltage waveforms for the proposed four-degree-of-freedom control method with four control variables v_f, d_1, d_2, φ.

(u_2) voltages are manipulated by the pulse-width-modulation (PWM) switching signals fed to the corresponding modules. Since the secondary side is connected to the grid with a direct-current (DC) to alternative-current (AC) converter, we call as the voltage from the H-Bridge side *grid-side voltage*. The voltage from the Flexbattery pack side is called as *Flexbattery-side voltage*.

Both signals u_1 and u_2 have the same frequency, with period T_{sw}. The amplitude of u_1 is denoted by v_f, and that of u_2 is v_g, as shown in Fig. 4. The duty cycles from the Flexbattery-side and the grid-side are d_1 and d_2, respectively. The phase shift between the fundamental components of u_1 and u_2 is φ. Note that $\varphi > 0$ means that the fundamental harmonic of u_1 is leading that of u_2 and vice-versa. Definitions of these symbols are summarized in Table I.

A. Inductor current calculation

The instantaneous inductor current at time t is given by

$$i_L(t) = \int_0^t \frac{u_1(\tau) - u_2(\tau)}{L}\,\mathrm{d}\tau + i_L(0), \tag{1}$$

where L is the inductance shown in Fig. 3, and $i_L(0)$ is the inductor's initial condition where $i_L(0) = 0$. The fundamental frequency of the inductor current is f_{sw}. By employing Fourier analysis, the mean square value of the inductor current in a switching period is given by

$$\begin{aligned} I_L^2 =& \frac{1}{T_{sw}} \int_0^{T_{sw}} i_L^2(t)\,\mathrm{d}t \\ =& \sum_{k=1,3,5,\ldots\infty}^{\infty} I_{L,k}^2, \end{aligned} \tag{2}$$

where $I_{L,k}$ is the root-mean-square (rms) value of the k^{th} harmonic component of the inductor current. According to [6] we have

$$\begin{aligned} I_{L,k}^2 = \frac{8}{\pi^2}\frac{1}{k^4 Z_L^2}\big(&v_f^2 \sin^2(\frac{k\pi}{2}d_1) + v_g^2 \sin^2(\frac{k\pi}{2}d_2) \\ &-2v_f v_g \sin(\frac{k\pi}{2}d_1)\sin(\frac{k\pi}{2}d_2)\cos(\frac{k\pi}{2}d_\phi)\big), \end{aligned} \tag{3}$$

with $Z_L = 2\pi f_{sw} L$ and $d_\phi = \dfrac{2\varphi}{\pi}$.

TABLE I: Symbol definition

Symbol	Definition
u_1	voltage from the Flexbattery-side
u_2	voltage from the grid-side
v_f	amplitude of the voltage u_1
v_g	amplitude of the voltage u_2
d_1	duty cycle of the voltage u_1
d_2	duty cycle of the voltage u_2
φ	phase shift between u_1 and u_2
d_ϕ	normalized phase shift defined by $d_\phi = \frac{2\varphi}{\pi}$
T_{sw}	switching period
f_{sw}	fundamental frequency, given by $f_{sw} = \frac{1}{T_{sw}}$
T_h	half switching period, given by $T_h = \frac{T_{sw}}{2}$
L	inductance
Z_L	inductor reactance at the fundamental frequency

B. Power flow regulation

The power transferred from u_1 to u_2 in a switching period is expressed by

$$p = \frac{1}{T_{sw}} \int_0^{T_{sw}} u_2(t) i_L(t)\,\mathrm{d}t. \tag{4}$$

The expression is expanded by Fourier analysis, and it is rewritten

$$p = \sum_{k=1,3,5,\ldots\infty}^{\infty} p_k, \tag{5}$$

where p_k is the power contributed by the k^{th} harmonic component. According to [6] we have

$$p_k = \frac{8 v_g v_f}{\pi^2 Z_L} \frac{\sin(\frac{k\pi}{2}d_1)\sin(\frac{k\pi}{2}d_2)\sin(\frac{k\pi}{2}d_\phi)}{k^3}. \tag{6}$$

C. Four-degree-of-freedom control

Compared to the triple-phase-shift control method, the proposed control scheme has one additional degree of freedom. The four control variables are: the amplitude of the voltage from the Flexbattery-side v_f, the duty cycles d_1 and d_2, and the normalized phase shift d_ϕ. The power transferred from the Flexbattery-side to the grid-side is regulated by these four control variables. A desired power transfer can be achieved by various combinations of (v_f, d_1, d_2, d_ϕ), unless it is out of the converter's operation range.

Nevertheless, these four control variables cannot be completely freely chosen but are subject to constraints in practice. Because we are focussing on the case where energy flows from the Flexbattery-side to the grid-side, the normalized phase shift meets the inequality $0 \leq d_\phi \leq 1$. Due to the physical limit of the Flexbattery pack, the voltage amplitude v_f is restricted to a close range set. The duty cycles d_1 and d_2 vary between 0 and 1.

III. Optimization control

A. Problem statement

The degrees of freedom in these four variables can be used to minimize the conduction losses in the converter while ensuring a desired power transfer. The conduction losses are proportional to the mean square value of the inductor current, and therefore the optimization objective is to minimize the value of the rms inductor current. The problem is formulated as

$$\begin{aligned} &\textit{minimize} \\ &\quad I_L^2(v_f, d_1, d_2, d_\phi), \\ &\textit{subject to} \\ &\quad p(v_f, d_1, d_2, d_\phi) = p^* \\ &\quad 0 \leq v_f \leq V_{f,max}, \\ &\quad 0 \leq d_1 \leq 1, \\ &\quad 0 \leq d_2 \leq 1, \\ &\quad 0 \leq d_\phi \leq 1, \end{aligned} \tag{7}$$

where p^* is the set-point for power, $V_{f,max}$ the maximum voltage level the Flexbattery pack can generate, and I_L^2 and p are given by (2) and (5), respectively.

B. Optimization problem approximation

It is challenging to find the analytical solution to the problem addressed in (7) due to its complexity, e.g. an infinite number of harmonics. Therefore, approximations are assumed as conventionally [11].

1) Power approximation: to simplify the calculation, only the fundamental harmonics are taken into account. The first order components of u_1 and u_2 are represented by phasors $\mathbf{v_1}$ and $\mathbf{v_2}$, respectively, as drawn in a phase-amplitude map in Fig. 5, where the fundamental inductor current $\mathbf{i_{L,1}}$ is also included. The rms values of $\mathbf{v_1}$ and $\mathbf{v_2}$ are given by

$$\begin{aligned} V_1 =& \frac{2\sqrt{2}}{\pi} \sin(\frac{\pi}{2} d_1) v_f, \\ V_2 =& \frac{2\sqrt{2}}{\pi} \sin(\frac{\pi}{2} d_2) v_g, \end{aligned} \tag{8}$$

respectively. Therefore, the power transferred from the Flexbattery-side to the grid-side is found to be, according to (6),

$$\begin{aligned} p \approx p_1 =& \frac{V_1 V_2}{Z_L} \sin(\frac{\pi}{2} d_\phi) \\ =& \frac{8 v_g v_f}{\pi^2 Z_L} \sin(\frac{\pi}{2} d_1) \sin(\frac{\pi}{2} d_2) \sin(\frac{\pi}{2} d_\phi). \end{aligned} \tag{9}$$

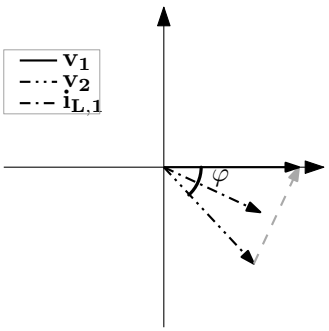

Fig. 5: Phasor diagram of the signals at fundamental frequency f_{sw}.

2) Inductor current approximation: The inductor current is approximated by taking into account the first and third harmonics only. As a result, it is given by

$$I_L^2 \approx I_{L,1}^2 + I_{L,3}^2, \tag{10}$$

where $I_{L,1}, I_{L,3}$ are given by (3).

C. Solve optimization problem

Therefore, the optimization problem in (7) is simplified to

$$\begin{aligned} &\textit{minimize} \\ &\quad \mathcal{F} = \sum_{k=1,3} I_{L,k}^2(v_f, d_1, d_2, d_\phi), \\ &\textit{subject to} \\ &\quad p_1(v_f, d_1, d_2, d_\phi) = p^* \\ &\quad 0 \leq v_f \leq V_{f,max}, \\ &\quad 0 \leq d_1 \leq 1, \\ &\quad 0 \leq d_2 \leq 1, \\ &\quad 0 \leq d_\phi \leq 1, \end{aligned} \tag{11}$$

where $\mathcal{F}$ is the optimization objective. Since it is quite difficult to find the solution of the problem stated in (11) in closed form, e.g. by solving differential equations, we adopt the brute-force approach to find the optimal solution.

It is done in this way: list all the feasible solutions (with certain resolution) for (v_f, d_1, d_2, d_ϕ) that meet the constraints, compare the corresponding results and select the one leading to the lowest value of $\mathcal{F}$. Note that different combinations of (v_f, d_1, d_2, d_ϕ) could lead to the same $\mathcal{F}$. In that case the optimal solution is selected randomly among those combinations. The optimization control can be easily implemented by creating a big lookup table indexed by the desired power off-line. The table becomes smaller when the resolution is lowered, but it can be interpolated in 4 dimensions.

IV. Converter Specification

From the previous discussion, one can expect that the optimal solution $(v_f', d_1', d_2', d_\phi')$ depends on the set-point for the power, the grid instantaneous voltage, the reactance of the inductor, and the maximum voltage level the Flexbattery pack can provide.

A. Converter specifications

The specifications of the power converter are given:

- Average power injected to Grid: $P_g = 1000\,\mathrm{W}$
- Grid power factor: assumed unity
- Grid rms voltage: $V_g = 220\,\mathrm{V}$
- Grid frequency: $f_g = 50\,\mathrm{Hz}$
- Maximum voltage from Flexbattery pack: $V_{f,max} = 400\,\mathrm{V}$.

The switching frequency is assumed to be far higher than that of the grid, hence the grid power and voltage are regarded unchanged during a switching period. According to the converter specifications, the instantaneous grid voltage and the set-point for the power are given by

$$\begin{aligned} v_g &= \sqrt{2}V_g \sin(2\pi f_g t), \\ p^* &= 2P_g \sin^2(2\pi f_g t), \end{aligned} \tag{12}$$

where t is the time.

B. Inductor reactance selection

According to (9), we can see that the instantaneous power transfer reaches its maximum value when the four variables (v_f, d_1, d_2, d_ϕ) are at their maximum. We define the maximum power the converter can transfer at time t is p_{max}, given by

$$p_{max} = p(v_f, d_1, d_2, d_\phi)|_{v_f = V_{f,max}, d_1 = 1, d_2 = 1, d_\phi = 1}. \tag{13}$$

Substituting (13) and (12) into (9), we have

$$\begin{aligned} p_{max} &= \frac{8 v_g V_{f,max}}{\pi^2 Z_L} \\ &= \frac{8\sqrt{2} V_g V_{f,max}}{\pi^2 Z_L} \sin(2\pi f_g t), \end{aligned} \tag{14}$$

which indicates that p_{max} is inversely proportional to the inductor reactance Z_L. To ensure a valid power transfer, the power set-point should be not bigger than the maximum power the converter can transfer, namely $p^* \leq p_{max}$. Therefore, by comparing (12) and (14) we get the inequality

$$Z_L \leq Z_{L,max}, \tag{15}$$

where $Z_{L,max} = \dfrac{8}{\pi^2} \dfrac{\sqrt{2} V_g V_{f,max}}{2P_g}$. The inductor reactance is chosen at its maximum value, given by

$$Z_L = Z_{L,max}. \tag{16}$$

V. Simulation results

An optimization simulation is performed over half a grid period. Fig. 6 shows the curves for the power set-point and the maximum power the converter can transfer. When $p^* < p_{max}$, there exist countless feasible (not necessarily optimal) solutions to the problem described in (11). When $p^* = p_{max}$, the solution is given by $v_f' = V_{f,max}$, $d_1' = 1$, $d_2' = 1$, $d_\phi' = 1$.

A. Optimization Plot

The optimal solution $(v_f', d_1', d_2', d_\phi')$ is found by employing the method explained in section III-C. The results are plotted in Fig. 7 and Fig. 8, where the former one displays the voltage value, and the latter one shows the duty cycles and the normalized phase shift. By substituting the obtained optimal solution into (11), the sum of the mean square value of the inductor currents at first and third order is obtained, as plotted in Fig. 9, denoted by $\mathcal{F}'$.

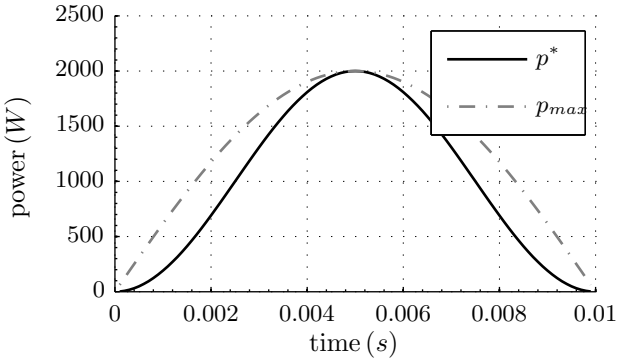

Fig. 6: The waveforms of the power set-point p^* and the maximum instantaneous power the converter can transfer p_{max}.

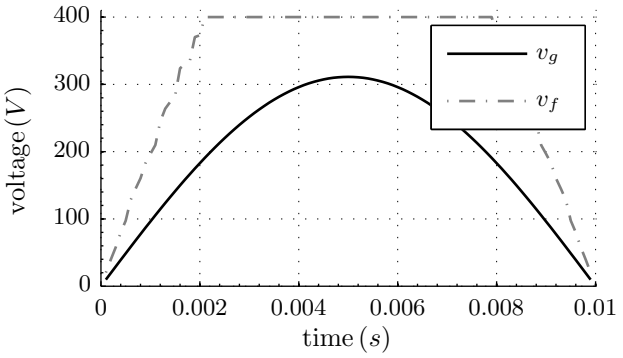

Fig. 7: Four-degree-of-freedom control optimization plot: voltages over half a grid period.

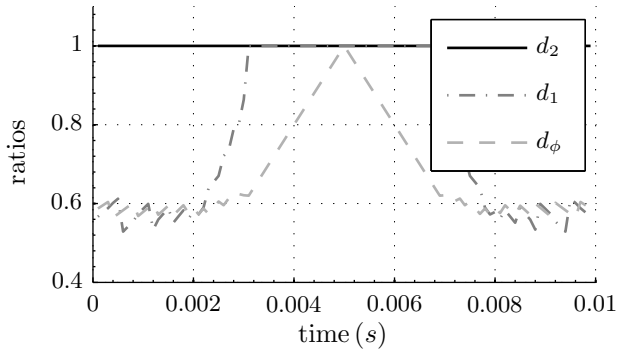

Fig. 8: Four-degree-of-freedom control optimization plot: d_1, d_2, d_ϕ over half a grid period.

B. Single degree of freedom control strategies

To show the merits of using all four degrees of freedom, it is interesting to look at other options that have a single degree of freedom. We compare their effectiveness with the proposed scheme regarding the mean square value of the inductor current.

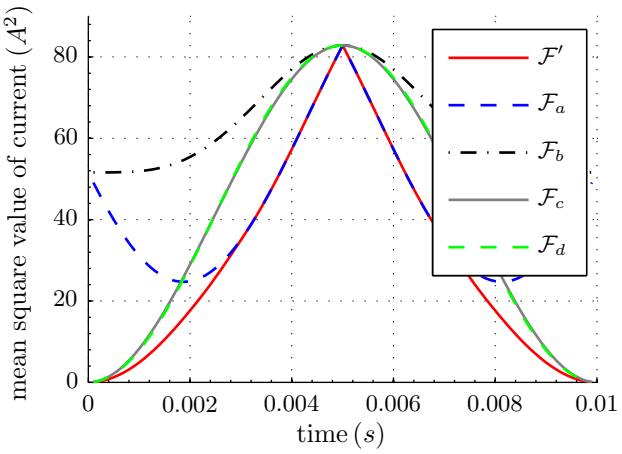

Fig. 9: The waveforms of the resulting mean square value of the current over half a grid period: solid red trace, proposed strategy; dashed blue trace, strategy a; dash-dot black trace, strategy b; solid grey trace, strategy c, dashed green trace, strategy d.

1) strategy a: It is pre-chosen that $v_f = V_{f,max}, d_1 = 1$ and $d_2 = 1$. Consequently, the normalized phase shift d_ϕ is defined by the desired power. The resulting mean square value of the inductor current is plotted in Fig. 9, as denoted by symbol $\mathcal{F}_a$.

2) strategy b: It is pre-chosen that $v_f = V_{f,max}, d_1 = 1, d_\phi = 1$. Consequently, the duty cycle d_2 is defined by the desired power. The resulting mean square value of the inductor current is plotted in Fig. 9, as denoted by symbol $\mathcal{F}_b$.

3) strategy c: It is pre-chosen that $v_f = V_{f,max}, d_2 = 1, d_\phi = 1$. Consequently, the duty cycle d_1 is defined by the desired power transfer. The resulting mean square value of the inductor current is plotted in Fig. 9, as denoted by symbol $\mathcal{F}_c$.

4) strategy d: It is pre-chosen that $d_1 = 1, d_2 = 1, d_\phi = 1$. Consequently, the voltage amplitude from the Flexbattery-side v_f is defined by the desired power transfer. The resulting mean square value of the inductor current is plotted in Fig. 9, as denoted by symbol $\mathcal{F}_d$.

C. TPS and DPS control strategies

1) When the inductor reactance is at its maximum: Another interesting comparison is that of traditional triple-phase-shift (TPS) and dual-phase-shift (DPS) with the proposed four-degree-of-freedom control method.

Triple-phase-shift [5] is obtained when the amplitude of the primary voltage is fixed. Here, we set the amplitude $v_f = V_{f,max}$. Solving the problem stated in (11) with an additional constraint $v_f = V_{f,max}$, we can get the optimal solution of

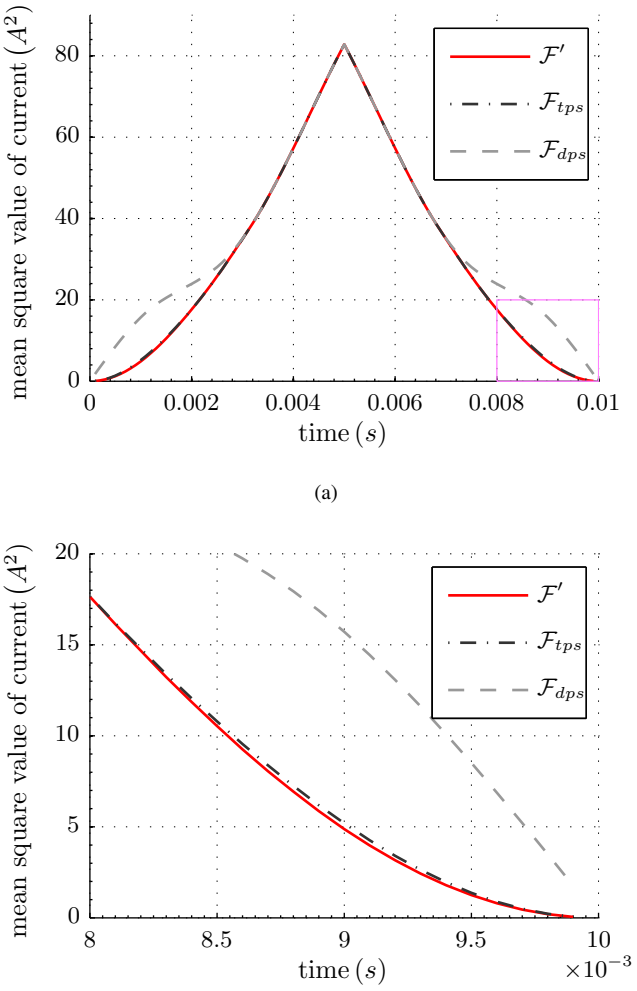

(a)

(b)

Fig. 10: Comparison of the proposed control method, TPS and DPS: (a) results over half a grid period; (b) zoomed results of the bold pink square indicated in (a).

TPS. The mean square value of the inductor current for TPS is plotted in Fig. 10, denoted by $\mathcal{F}_{tps}$.

Similarly, dual-phase-shift (DPS) [4] is obtained when we set the primary and secondary voltages to have the same duty cycles, in addition to a fixed amplitude. Therefore, solving the problem stated in (11) with two additional constraints $v_f = V_{f,max}$ and $d_1 = d_2$ yields the optimal solution of DPS. The mean square value of the inductor current for DPS is plotted in Fig. 10, denoted by $\mathcal{F}_{dps}$.

2) When the inductor reactance is halved: The maximum power the converter can transfer is doubled correspondingly according to (9). As a result, the converter will not always be used at its full power. Fig. 11 shows the results of the proposed control method, TPS and DPS when the inductor reactance is halved.

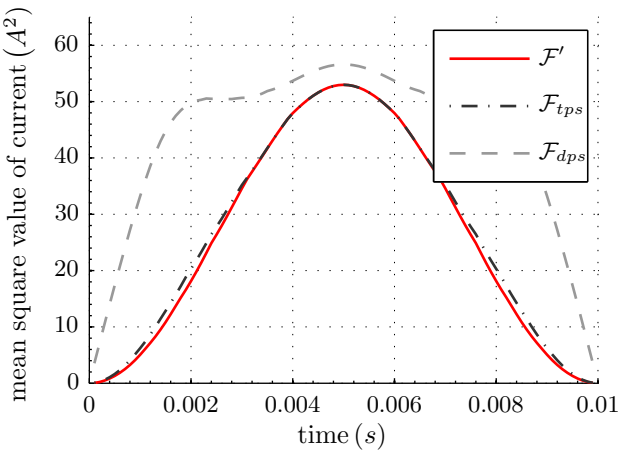

Fig. 11: Comparison of the proposed control method, TPS and DPS when $Z_L = 0.5Z_{L,max}$: results over half a grid period;

VI. Discussion and Conclusion

Compared to the triple-phase-control scheme, the four-degree-of-freedom control approach includes one more degree of freedom for control. The additive benefit is that the rms inductor current can be minimized further by taking into account third or higher-order harmonics. The proposed scheme leads to the lowest rms inductor current with comparison to single degree of freedom control strategies, triple-phase-shift and dual-phase-shift, as shown in Fig. 9 and Fig. 10.

The results in section V imply that the optimal control strategy tends to decrease the phase shift angle. Due to the limited operating range of the Flexbattery pack, the voltage and the duty cycle from the Flexbattery-side are clamped at their maximum limits when $0.003s < t < 0.007s$, as they are shown in Fig. 7 and Fig. 8. During this time span, the proposed control scheme leads to the same result as the strategy a presented in section V-B. Another trend we can see from the results is that the optimal control strategy attempts to balance the voltages and duty cycles from Flexbattery and grid sides, as shown in Fig. 7 and Fig. 8. A design which differs these voltage values or duty cycles increases the mean square value of the inductor current, as $\mathcal{F}_a$ and $\mathcal{F}_b$ are shown in Fig. 9.

In DPS the voltage from the Flexbattery-side is significantly different from the grid-side when the grid voltage approaches zero, hence the mean square value of the inductor current of DPS is higher than the proposed control method, as shown in Fig. 10. When the inductor reactance is chosen at its maximum value the benefit of the proposed method is not significant compared to TPS (Fig. 10) because the converter needs to use its full power, leaving it less freedom to optimize the four variables. The benefit is more significant when the inductor reactance is chosen at its half maximum value (Fig. 11). The reason is that the four control variables do not necessarily operate close to their boundaries, leaving more space for optimization.

In conclusion, this paper proposes a four-degree-of-freedom control method and compares its performance with other strategies regarding the circulating current. The circulating current can be minimized by applying the proposed control method, decreasing the overall conduction losses. The proposed method can be easily implemented by creating a look-up table off-line. Compared to TPS, the added one degree of freedom can be also used to facilitate zero-voltage-switching operation.

Acknowledgement

The project is founded by the *Dutch Technology and Science Foundation-STW*, affiliated with the project called *"New energy conversion, storage and distribution technologies for smart buildings"*. The authors would like to acknowledge the help from the staff of the Electromechanics and Power Electronics group at Eindhoven University of Technology.

References

[1] B. J. D. Vermulst, J. L. Duarte, C. G. E. Wijnands, and E. A. Lomonova, "Single-stage three-phase AC to DC conversion with isolation and Bi-directional power flow," in *IECON 2014 - 40th Annual Conference of the IEEE Industrial Electronics Society*, Oct. 2014, pp. 4378–4383.

[2] H. Tao, A. Kotsopoulos, J. L. Duarte, and M. A. M. Hendrix, "A Soft-Switched Three-Port Bidirectional Converter for Fuel Cell and Supercapacitor Applications," in *2005 IEEE 36th Power Electronics Specialists Conference*, Jun. 2005, pp. 2487–2493.

[3] R. W. A. A. D. Doncker, D. M. Divan, and M. H. Kheraluwala, "A three-phase soft-switched high-power-density dc/dc converter for high-power applications," *IEEE Transactions on Industry Applications*, vol. 27, no. 1, pp. 63–73, Jan 1991.

[4] H. Bai and C. Mi, "Eliminate reactive power and increase system efficiency of isolated bidirectional dual-active-bridge dc-dc converters using novel dual-phase-shift control," *IEEE Transactions on Power Electronics*, vol. 23, no. 6, pp. 2905–2914, Nov 2008.

[5] Y. A. Harrye, K. H. Ahmed, G. P. Adam, and A. A. Aboushady, "Comprehensive steady state analysis of bidirectional dual active bridge dc/dc converter using triple phase shift control," in *Industrial Electronics (ISIE), 2014 IEEE 23rd International Symposium on*, June 2014, pp. 437–442.

[6] J. Huang, Y. Wang, Z. Li, and W. Lei, "Unified triple-phase-shift control to minimize current stress and achieve full soft-switching of isolated bidirectional dc-dc converter," *IEEE Transactions on Industrial Electronics*, vol. 63, no. 7, pp. 4169–4179, July 2016.

[7] E. Lemmen, J. L. Duarte, and E. A. Lomonova, "Flexbattery - merging multilevel power conversion and energy storage," in *Proc. IEEE Energy Convers. Congr. Expo.*, Sept 2016.

[8] E. Lemmen, J. L. Duarte, M. C. M. Drabbe, and J. R. G. Maar, "Flexbattery," United States of America Provisional Patent 62/263 145, Dec 4, 2015.

[9] E. Lemmen, J. van Duivenbode, J. L. Duarte, and E. A. Lomonova, "Flexible multilevel converters using four-switch extended commutation cells," vol. 3, no. 3, pp. 794–804, Sept 2015.

[10] E. Lemmen and J. L. Duarte, "4-switch extended commutation cell," United States of America Patent 14/935 059, Nov 6, 2015.

[11] F. Krismer and J. W. Kolar, "Closed form solution for minimum conduction loss modulation of dab converters," *IEEE Transactions on Power Electronics*, vol. 27, no. 1, pp. 174–188, Jan 2012.